Mon. Not. R. Astron. Soc. **000**, 1–14 (2015) Printed July 10, 2015 (MN LATEX style file v2.2)

Energy dependence of the band-limited noise in black hole X-ray binaries⋆

H. Stiele † ‡, W. Yu
Shanghai Astronomical Observatory and Center for Galaxy and Cosmology, 80 Nandan Road, Shanghai, 200030, China

2015 July 7

arXiv:1412.3547v2 [astro-ph.HE] 9 Jul 2015

ABSTRACT
Black hole low-mass X-ray binaries show a variety of variability features, which manifest themselves as narrow peak-like structures superposed on broad noise components in power density spectra in the hard X-ray emission. In this work we study variability properties of the band-limited noise component during the low-hard state for a sample of black hole X-ray binaries. We investigate the characteristic frequency and amplitude of the band-limited noise component and study covariance spectra. For observations that show a noise component with a characteristic frequency above one Hz in the hard energy band (4 – 8 keV) we found this very same component at a lower frequency in the soft band (1 – 2 keV). This difference in characteristic frequency is an indication that while both the soft and the hard band photons contribute to the same band-limited noise component, which likely represents the modulation of the mass accretion rate, the soft photons origin actually further away from the black hole than the hard photons. Thus the soft photons are characterized by larger radii, lower frequencies and softer energies, and are probably associated with a smaller optical depth for Comptonisation up-scattering from the outer layer of the corona, or suggesting of a temperature gradient of the corona. We interpret this energy dependence within the picture of energy-dependent power density states as a hint that the contribution of the up-scattered photons originating in the outskirts of the Comptonising corona to the overall emission in the soft band is becoming significant.

Key words: X-rays: binaries – X-rays: individual: H 1743–322, GX 339–4, XTE J1650–500, XTE J1752-223, Swift J1753.5-0127 – binaries: close – black hole physics

1 INTRODUCTION

Transient low-mass black hole X-ray binaries show distinct changes of their spectral and variability properties as they evolve during an outburst, that are interpreted as evidence for changes in the accretion flow and X-ray emitting regions. This behavior can be classified by different phenomenological states through which the black hole transient (BHT) evolves during an outburst (Remillard & McClintock 2006; Belloni 2010). At the beginning of a typical outburst BHTs are usually in the low hard state (LHS) where their power density spectra (PDS) are dominated by band-limited noise (BLN) on which narrow quasi-periodic features (quasi-periodic oscillations; QPOs) are superimposed. During the evolution through the LHS and into the hard intermediate state (HIMS) the amplitude as well as the centroid frequency of the QPOs increases. In the energy range covered by the RXTE/PCA detector (i. e. >2 keV) the PDS show a smooth transition from the LHS to the HIMS. This picture changes dramatically when softer energies are included, as they reveal the existence of two distinct power spectral states at soft and hard X-rays with the onset of the HIMS (Yu & Zhang 2013; Stiele & Yu 2014). The transition to the soft intermediate state (SIMS) is marked by the appearance of another type of QPO, and an overall fractional rms in the 5 – 10 per cent interval (Casella et al. 2005; Muñoz-Darias et al. 2011). In the high soft state (HSS) the variability is even lower and the PDS is dominated by power-law noise. After experiencing a substantial decrease in luminosity during the HSS the BHT returns back to the LHS again usually passing the HIMS and SIMS (Stiele et al. 2011a).

In the LHS the X-ray emission is very noisy and the fractional rms can reach values up to 40–50 per cent. The first detection of a difference in time scales between the soft and hard flux from a BHT was found in observations of the HIMS of GS 1124–68 and GX 339–4 obtained with Ginga (Belloni et al. 1997).The shape of the PDS, which is dominated by BLN, can be fitted with a combination of Lorentzian components (Belloni et al. 2002). Four main components have been identified ($0.001 < \nu <$ a few 100 Hz): a low-frequency one fitting the flat-top part, a peaked (some-

⋆ Based on observations obtained with *XMM-Newton*, an ESA science mission with instruments and contributions directly funded by ESA Member States and NASA.

† E-mail: hstiele@mx.nthu.edu.tw
‡ Institute of Astronomy and Department of Physics, National Tsing Hua University, No. 101 Sect. 2 Kuang-Fu Road, Hsinchu, 30013, Taiwan

© 2015 RAS

times QPO-like) component, and two broad Lorentzians at higher frequencies. These components are characterized by their characteristic frequency and by the amount of variability they contribute, where the latter one is measured as factional rms. Studying the fractional rms as a function of energy (the "rms spectrum") it was shown that it is either flat or decreases by a few per cent in the energy range covered by RXTE/PCA (Belloni et al. 2011, and references therein). This shape has been interpreted in the framework of Comptonization models (Gierliński & Zdziarski 2005). Using covariance spectra and ratios obtained from *XMM-Newton* data, an increased disc blackbody variability with respect to the Comptonized emission was detected below 1 keV at time scales longer than one second, while on shorter time scales the disc variability is driven by variability of the Comptonized component, consistent with propagating models modified by disc heating at short time scales (Wilkinson & Uttley 2009; Cassatella et al. 2012). In addition to the BLN component type-C QPOs (Wijnands et al. 1999; Motta et al. 2011) can be present. They can be observed over a relatively large range of frequencies – roughly from 0.01 to 30 Hz – and their fractional rms is of the oder of 3 – 15 per cent.

In recent years much work has gone into developing and exploring models to describe QPOs and noise components. An excellent summary of these models can be found in the extensive recent review of Belloni & Stella (2014, see also references therein). BLN can be explained within the "propagating fluctuation" model (Lyubarskii 1997), where variability is caused by variations in the mass accretion rate which propagate through the disc, so that shorter time-scale variations either from coronal flares or fluctuation in the mass accretion rate or similar processes in the inner parts of the disc are superimposed on longer time-scale variations from further out (e. g. Uttley & McHardy 2001). BLN is also seen in neutron star low mass X-ray binaries. Likely indicators of the orbital frequency in the innermost accretion flow such as the kHz QPO Frequency in neutron star low mass X-ray binaries are found to vary with the flux corresponding to the time scale of the BLN in a manner similar to that established for variability on longer time scales which is due to modulation in the mass accretion rate, providing an independent evidence that the BLN corresponds to the modulation in the mass accretion rate which causes changes in the inner edge or characteristic frequencies in the accretion flow (Cao & Yu 2009).

2 OBSERVATIONS AND DATA ANALYSIS

In this paper, we study the variability properties of the characteristic frequency and variability amplitude of the BLN in different energy bands during the LHS for a sample of BHTs. We used observations of GX 339–4, H 1743–322, XTE J1650–500, XTE J1752–223, and Swift J1753.5–0127. Details on the individual observations are given in Table 1. All observations were taken during the LHS. We filtered and extracted the pn event files, using standard SAS (version 13.0.0) tools, paying particular attention to extract the list of photons not randomized in time. For our study we selected the longest, continuous exposure available in each observation (see Table 1). We used the SAS task `epatplot` to investigate whether the observations are affected by pile-up, and in the case of pile-up excluded the column(s) with the highest count rate until the selection results in an observed pattern distribution that follows the theoretical prediction quite nicely. We selected single and double events (PATTERN<=4) for our study.

2.1 Timing analysis

We extracted power density spectra (PDS) in two different energy bands, namely 1 – 2 and 4 – 8 keV. After verifying that the noise level at frequencies above 30 Hz is consistent with the one expected for Poissonian noise (Zhang et al. 1995), we subtracted the contribution due to Poissonian noise, normalised the PDS according to Leahy et al. (1983) and converted to square fractional rms (Belloni & Hasinger 1990). The PDS were fitted with models composed of zero-centered Lorentzians for BLN components, and Lorentzians for QPOs. The resulting power spectra in the two energy bands thus contain only source variability and can be compared with each other.

In addition, we derived rms spectra for each component of the PDS using the amplitude (normalisation) of the Lorentzians. Furthermore, we derived covariance spectra following the approach described in Wilkinson & Uttley (2009). To study variability on shorter time scales we used 0.1 s time bins measured in segments of 4 s. For longer time scales 2.7 s time bins in segments of 270 s were used. As reference band we used the energy range between 1 and 4 keV, taking care to exclude energies from the reference band that are in the channel of interest.

2.2 Spectral analysis

We extracted energy spectra of all observations, using the RAWX values given in table 1 for the source spectra. To extract background spectra we used columns $3 \leqslant \mathrm{RAWX} \leqslant 5$. In the case of burst mode observations we used RAWY < 140 following the procedure outlined in Kirsch et al. (2006). We payed special attention to generate ARF files of the pile-up corrected source region, following the steps laid down in the *XMM-Newton* Users Guide. As it is known that energy spectra obtained form *XMM-Newton* EPIC-pn fast-readout modes can be affected by gain shift due to Charge-transfer inefficiency (CTI), which leads to an apparent shift of the instrumental edges visible at low energies, we also generated spectra applying the SAS task EPFAST to the data. Apart form the observation of H 1743–322 no significant changes between the energy spectra obtained with and without EPFAST are noticeable at low energies, and a residual feature at ∼2 keV, related to small shifts in energy gain at the Si-K and Au-M edges of the instrumental response, remains present in the data obtained with EPFAST (Kolehmainen et al. 2011). As there are no significant changes of the energy spectra at low energies and as EPFAST leads to an over-correction of the CTI at higher energies (see e. g. Walton et al. 2012; Stiele & Yu 2014), we fitted the spectra obtained without EPFAST and limited our spectral study to the 1 – 10 keV energy range.

3 RESULTS

3.1 Studying timing properties

Investigating the PDS of the individual sources in the two energy bands, we find that in general the overall shape of the components is consistent between the soft (1 – 2 keV) and hard (4 – 8 keV) band (see Fig. 1). For some observations, an additional QPO or peaked noise component is present in one of the two energy bands but missing in the other one. In order to study the shapes of the PDS in a more quantitative way, we determined the characteristic frequency, defined by $\nu_{\mathrm{max}} = \sqrt{\nu^2 + \Delta^2}$, where ν is the centroid frequency, and Δ is the half width at half maximum (Belloni et al. 2002), of

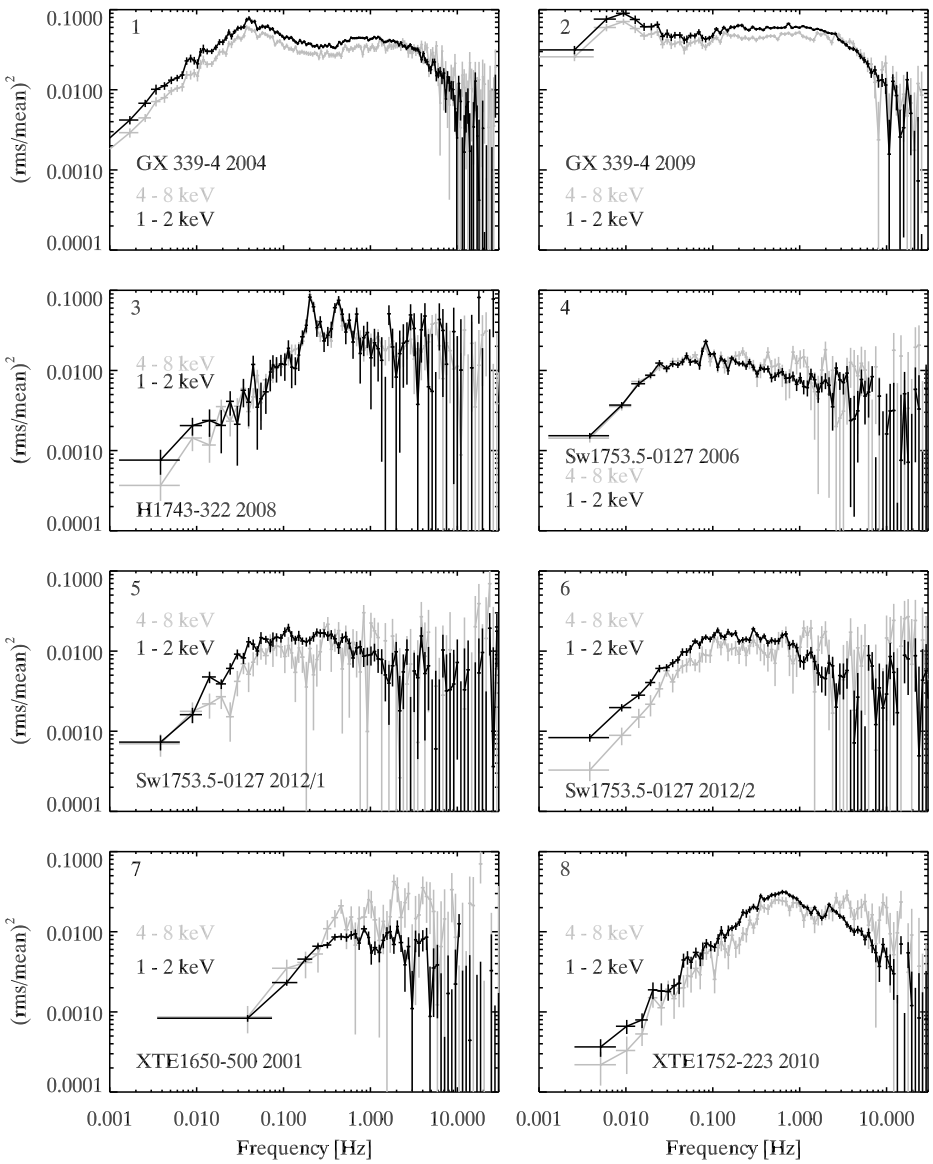

Figure 1. PDS of all eight observations in the soft (1 – 2 keV) and hard (4 – 8 keV) band. In observations where the characteristic frequency is at higher frequencies, the power in the hard band is systematically higher than the power in the soft band in the overall frequency range.

each component. In the case of BLN, where $\nu = 0$, the characteristic frequency equals the break frequency. A visualization of the different components fitted to the hard band PDS of GX 339–4 and named following the nomenclature used in Belloni et al. (2002) and Belloni & Stella (2014) can be found in Fig. 2. Figure 3 (see also Tab. 2) shows the characteristic frequency obtained in the soft band versus the one derived from the hard band. Apart from the 2006 observation of Swift J1753.5-0127 and the observation of H 1743–322, we detect at least one component for which the characteristic frequency obtained in the soft band is lower than the one obtained in the hard band. For the remaining noise components, the characteristic frequencies in both bands are equal within errors. In cases where the characteristic frequency in the soft band is lower than in the hard band, this is always true for the component with the highest characteristic frequency (L_l). Wilkinson & Uttley (2009) studied the variability of the 2004 observation of GX 339–4 and the 2006 observation of Swift J1753.5–0127 in the 0.5 – 1 keV and 2 – 10 keV bands. They reported qualitatively, without obtaining characteristic frequencies through fits of the PDS, that in the case of GX 339–4 the higher frequency component in the PDS appears "to be shifted to even higher frequencies in the hard band", while in the case of Swift J1753.5–0127 the "soft and hard PDS appear to overlap more closely at higher frequencies". In a study of the SMBH system Ark 564 a similar energy dependence of the characteristic frequency of the higher frequency component has been found, while the lower frequency component did not show any energy de-

Table 1. Details of *XMM-Newton* observations

#	Source	Obs. id.	Date	Mode‡	Net Exp. [ks]	Exp.† [ks]	RAWX*
1	GX 339–4	0204730201	2004 March 16	T	135.067	93.20	31 – 36 & 40 – 43
2	GX 339–4	0605610201	2009 March 26	T	33.529	32.234	31 – 37 & 39 – 45
3	H 1743–322	0554110201	2008 Sep. 29	T	22.148	13.5	32 – 35 & 39 – 44
4	Swift J1753.5–0127	0311590901	2006 March 24	T	41.948	40.643	31 – 45
5	Swift J1753.5–0127	0691740201	2012 Sep. 10	T	40.091	37.890	31 – 36 & 39 – 45
6	Swift J1753.5–0127	0694930501	2012 Oct. 08	T	30.938	28.740	31 – 36 & 39 – 45
7	XTE J1650–500	0136140301	2001 Sep. 13	B	24.947	23.201	30 – 44
8	XTE J1752–223	0653110101	2010 April 06	T	41.917	19.700	30 – 46

Notes:
‡: T for timing mode, B for burst mode
†: exposure used in this study
*: detector columns from which source photons have been selected

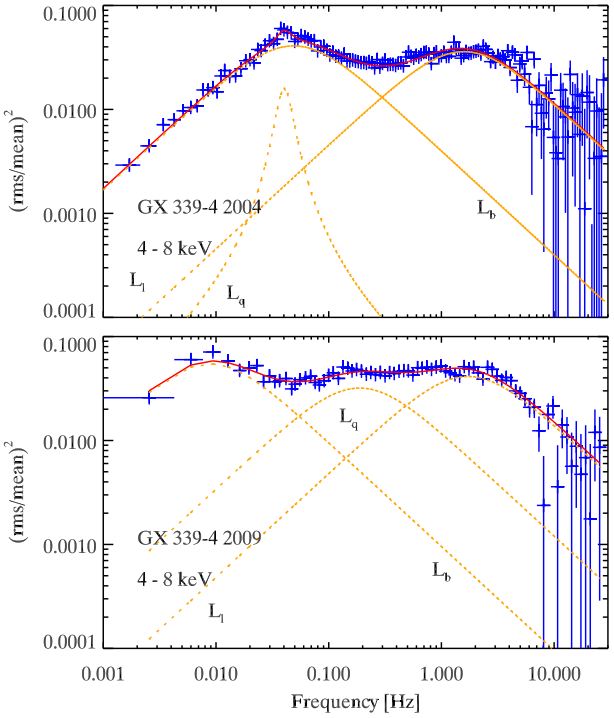

Figure 2. PDS of the 2004 (upper panel) and 2009 (lower panel) observations of GX 339-4 in the hard (4 – 8 keV) band to visualise the individual components (dashed orange lines). They are named following the nomenclature used in Belloni et al. (2002) and Belloni & Stella (2014). The component named L_q can be peaked (like in the upper panel) or broad (lower panel). For observations that only require two components to obtain decent fits the component L_q is not needed (which is the case for all observations of Swift J1753.5-0127; see Tab. 2).

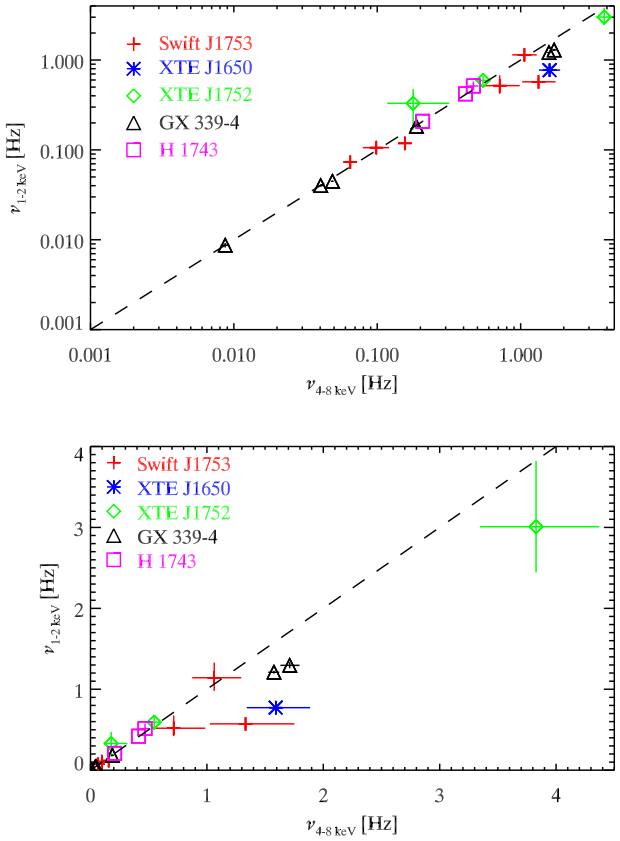

Figure 3. Characteristic frequency of the PDS components in the soft (1 – 2 keV) versus hard (4 – 8 keV) band, on double-logarithmic (upper panel) and linear scale (lower panel). The dashed line indicates equal frequencies. For almost all observations we find at least one data point which lies below the dashed line, i. e. that we find one component for which the characteristic frequency obtained in the soft band is lower than the one obtained in the hard band. For the remaining noise components, the characteristic frequencies in both bands are equal within errors. Different symbols indicate individual sources.

pendence between the 0.6 – 2 and 2 – 10 keV bands (McHardy et al. 2007). XTE J1753-223 that has been observed during outburst decay shows the highest break frequency and rather big error bars. A clear energy dependence of the characteristic frequency can be seen in the four observations that show break frequencies between 1 and 2 Hz in the hard band.

To rule out the possibility that the change of the characteristic

Table 2. List of characteristic frequencies for all observations in both energy bands.

#	Source	$\nu_{1-2\mathrm{keV}}$	$\nu_{4-8\mathrm{keV}}$	L†
1	GX 339–4	1.21 ± 0.02	1.58 ± 0.05	L_l
1	GX 339–4	$4.47 \pm 0.07 \times 10^{-2}$	$4.87 \pm 0.10 \times 10^{-2}$	L_b
1	GX 339–4	$0.40 \pm 0.01 \times 10^{-1}$	$0.40 \pm 0.02 \times 10^{-1}$	L_q
2	GX 339–4	1.30 ± 0.04	1.71 ± 0.08	L_l
2	GX 339–4	0.18 ± 0.01	0.19 ± 0.01	L_q
2	GX 339–4	$0.87 \pm 0.05 \times 10^{-2}$	$0.87 \pm 0.06 \times 10^{-2}$	L_b
3	H 1743–322	$0.51^{+0.06}_{-0.05}$	0.49 ± 0.04	L_l
3	H 1743–322	$4.20^{+0.11}_{-0.08} \times 10^{-1}$	$4.12^{+0.04}_{-0.02} \times 10^{-1}$	L_{qh}
3	H 1743–322	$2.08^{+0.02}_{-0.03} \times 10^{-1}$	$2.07 \pm 0.02 \times 10^{-1}$	L_q
4	Swift 1753.5–0127	$1.14^{+0.19}_{-0.16}$	$1.06^{+0.23}_{-0.19}$	L_l
4	Swift 1753.5–0127	$0.73 \pm 0.03 \times 10^{-1}$	$0.65 \pm 0.04 \times 10^{-1}$	L_b
5	Swift 1753.5–0127	$0.52^{+0.16}_{-0.10}$	$0.71^{+0.27}_{-0.18}$	L_l
5	Swift 1753.5–0127	0.11 ± 0.01	0.10 ± 0.02	L_b
6	Swift 1753.5–0127	$0.57^{+0.07}_{-0.06}$	$1.33^{+0.42}_{-0.31}$	L_l
6	Swift 1753.5–0127	0.12 ± 0.01	0.16 ± 0.02	L_b
7	XTE 1650–500	0.77 ± 0.04	$1.59^{+0.30}_{-0.25}$	L_l
8	XTE J1752–223	$3.01^{+0.81}_{-0.56}$	$3.83^{+0.54}_{-0.48}$	L_l
8	XTE J1752–223	$0.59^{+0.07}_{-0.09}$	0.55 ± 0.06	L_q
8	XTE J1752–223	$0.33^{+0.14}_{-0.16}$	$0.18^{+0.14}_{-0.06}$	L_b

Notes:
L†: PDS component: L_l, L_q, and L_b are used in the way shown in Fig. 2, while L_{qh} denotes the harmonic of the QPO

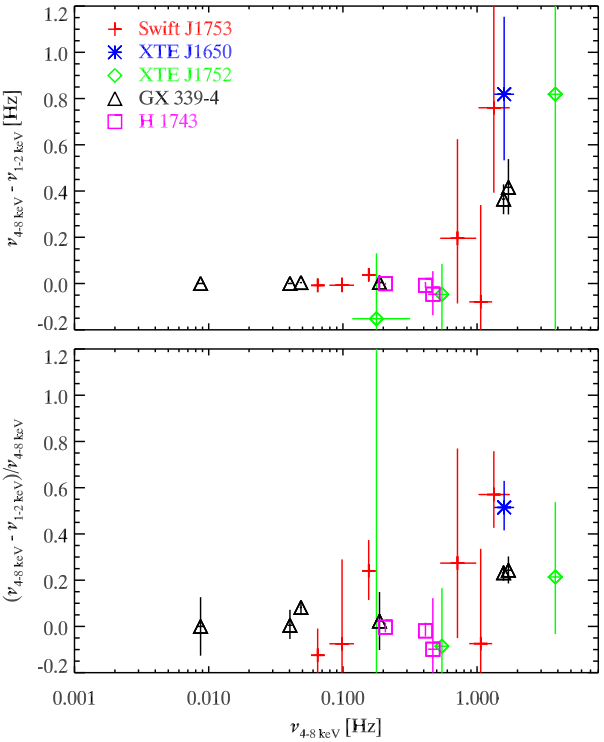

Figure 4. Absolute (upper panel) and relative (lower panel) change of the characteristic frequency between the hard and soft band versus the frequency in the hard band. Different symbols indicate individual sources.

frequency is mimicked by the emergence of a type-C QPO in the hard band, we added an additional Lorentzian to the fits of the hard band PDS and redetermined the characteristic frequencies. The allowed frequency range for the added Lorentzian was obtained from the relation of characteristic frequency and centroid QPO frequency presented in Fig. 11 of Belloni et al. (2002). For each observation, we used the lowest characteristic frequency found in the soft band to select the range of allowed centroid QPO frequencies. In addition the added Lorentzian had to be narrow. We found that the changes of the characteristic frequency caused by the added Lorentzian are within the errors of the values without added component. We estimated the significance of the added Lorentzian from its normalisation. This showed that the added Lorentzian is not significant at all ($0.7 - 1.4\ \sigma$).

We also checked for the presence of additional disc variability at low frequencies in the soft band by adding a power law component to the model used to fit the PDS. A power law component was used to test for disc variability, as in the HSS, which is dominated by emission of the accretion disc, the PDS is consistent with power law noise at all frequencies (see e. g. Miyamoto et al. 1994; Cui et al. 1997; Churazov et al. 2001; Remillard & McClintock 2006; Belloni 2010). In all observations fitting returned the normalisation of the power law component as zero, which implies that none of the PDS shows additional disc variability at low energies.

In Fig. 4 we show the difference in the characteristic frequency between the hard and soft band, determined by $\delta\nu_{\mathrm{max}} = \nu_{\mathrm{max;4-8keV}} - \nu_{\mathrm{max;1-2keV}}$, versus the characteristic frequency in hard band. As can be seen from Fig. 4 there is no clear correlation between the change of the characteristic frequency and the characteristic frequency itself. Using the characteristic frequency in the softer band instead of the one from the hard band on the x-axis leads to a shift to lower frequencies by $\delta\nu_{\mathrm{max}}$ for points with $\delta\nu_{\mathrm{max}} > 0$ and to higher frequencies for those with $\delta\nu_{\mathrm{max}} < 0$. In addition, Fig. 4 also shows the relative changes of the characteristic frequency, defined as $\delta\nu/\nu_{\mathrm{max;4-8keV}}$ versus the characteristic frequency in hard band. Again no clear correlation between the parameters shown can be seen.

In addition to the energy dependence of the characteristic frequency, we investigate the energy dependence of the variability amplitude of the BLN. The rms spectra of all PDS components are shown in Fig. 5. The BLN component with the highest characteristic frequency (L_l) is indicated by (red) crosses. In the observations of GX 339–4, H 1743–322, and the September 2012 observation of Swift J1753.5–0127 this component does not show a strong energy dependence and it is either rather flat or slowly decreasing with increasing energy. This behaviour of the rms spectra has been observed in the hard state observations presented in Gierliński & Zdziarski (2005). The remaining two observations of Swift J1753.5–0127 show a jump in variability around 4 – 5 keV, while variability remains rather constant at lower and higher energies. A behaviour observed in the hard intermediate state (Gierliński & Zdziarski 2005). The observations of XTE J1650–500 and XTE J1752–223 show much lower variability in the 1 – 2 keV band compared to the rather constant variability above 2 keV.

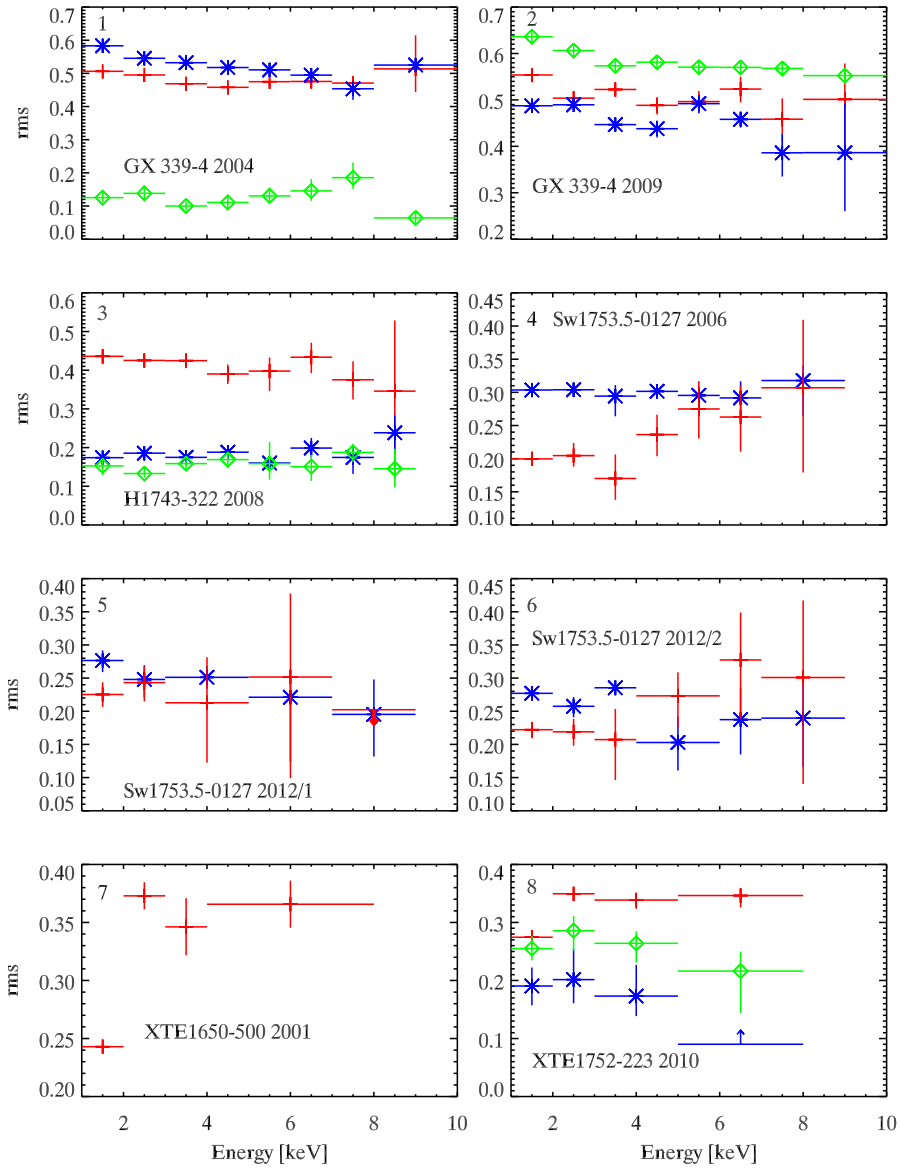

Figure 5. Rms spectra of all eight observations. Different symbols (colours) indicate different components of the PDS. The BLN component with the highest characteristic frequency (L_l) is indicated by (red) crosses. The BLN component with the lowest characteristic frequency (L_b) is indicated by (blue) stars, and the intermediate component (L_b) is indicated by (green) diamonds, expect for H 1743–322 where the QPO and its harmonic are indicated by (blue) stars and (green) diamonds, respectively.

3.2 Including energy spectra

We performed our investigation of the *XMM-Newton*/EPIC-pn energy spectra within ISIS V. 1.6.2 (Houck & Denicola 2000) in the 1 – 10 keV energy range, taking into account a systematic error of 1%. To obtain comparable spectral parameters, we fitted all spectra with the same model consisting of an absorbed disc blackbody plus thermal Comptonisation component (NTHCOMP; Zdziarski et al. 1996; Życki et al. 1999), including a high-energy cut-off. The foreground absorption is modeled with TBABS (Wilms et al. 2000) and the values of n_H are taken from the literature: $n_H = 7.8{\times}10^{21}$ cm^{-2} for XTE J1650–500 (Miller et al. 2002), $n_H = 2.3{\times}10^{21}$ cm^{-2} for Swift J1753.5–0127 (Mostafa et al. 2013), $n_H = 5.0{\times}10^{21}$ cm^{-2} for GX 339–4 (Zdziarski et al. 2004), $n_H = 7.2{\times}10^{21}$ cm^{-2} for XTE J1752–223 (Stiele et al. 2011b) and $n_H = 1.6{\times}10^{22}$ cm^{-2} for H 1743–322 (Capitanio et al. 2009). The temperature at the inner edge of the accretion disc is taken as temperature of the seed photons for the Comptonised component. In addition, a gaussian is added to model the residual visible in all observations at ~2 keV (see Sect. 2.2). In the case of GX 339–4 a second gaussian is need to fit the Fe-emission line at 6.4 keV. In the case of H 1743–322 we used the data with correction of CTI effects at low energies, and

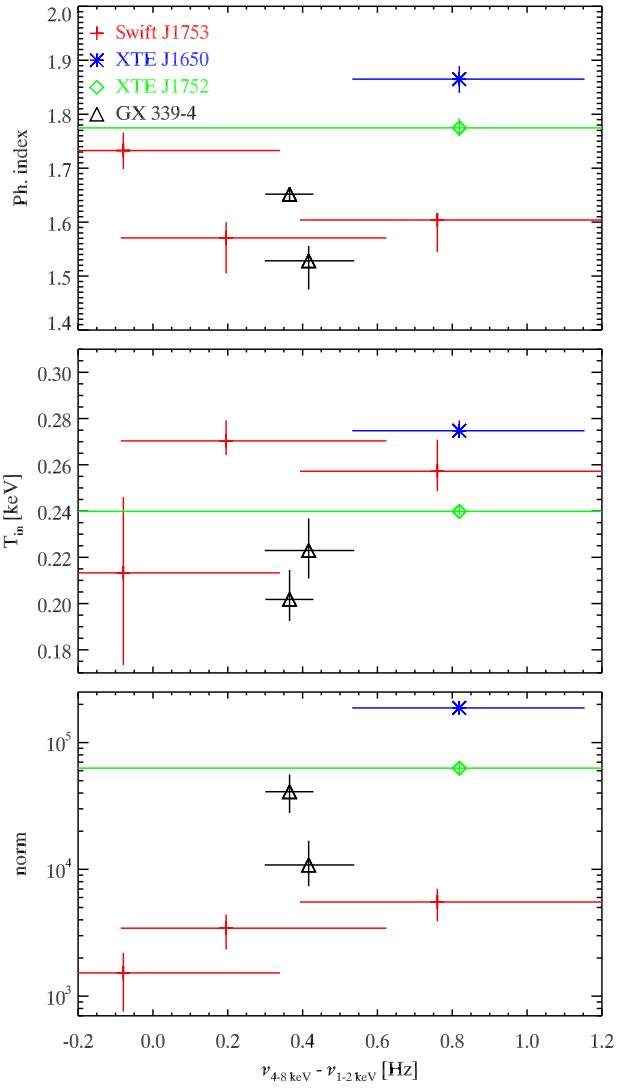

Figure 6. Behaviour of the photon index (upper panel), inner disc temperature (middle panel) and normalization of the disc component (lower panel) depending on the difference in the characteristic frequency $\delta\nu_{\rm max}$ of the component with the highest characteristic frequency. Different symbols indicate individual sources.

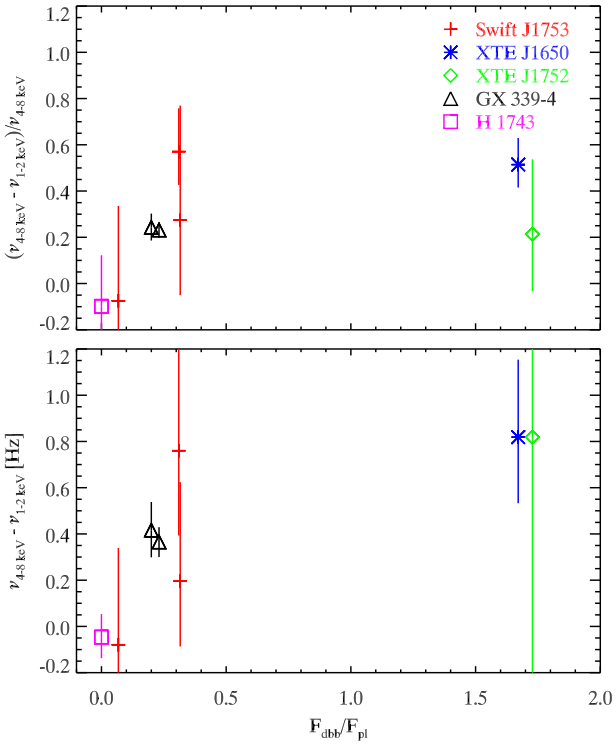

Figure 7. Absolute (upper panel) and relative (lower panel) change of the characteristic frequency between the hard and soft band of the component with the highest characteristic frequency versus the ratio of the flux contributed by the disc emission to the one of the Comptonized emission in the 1 – 2 keV band. Different symbols indicate individual sources.

fitted those with the same model that has been used for GX 339–4. For H 1743–322 the obtained fit implies a large disc normalization ($\sim 5 \times 10^8$) and a very low inner edge temperature ($\sim 10^{-3}$keV). A more detailed study of the spectrum showed that the disc blackbody component is not need to obtain a decent fit. Hence, we removed this component, and fixed the seed temperature for the Comptonization model at the disc temperature mentioned above.

Figure 6 shows the behaviour of the photon index, inner disc temperature and normalization of the disc component depending on the difference in the characteristic frequency $\delta\nu_{\rm max}$ of the component with the highest characteristic frequency. The values for H 1743–322 are omitted in this figure as no disc component was need to obtain an acceptable fit for this source. For the three observations of Swift J1753.5-0127 a slide increase in the disc normalization with increasing $\delta\nu_{\rm max}$ is visible. This behaviour is not observed in the two observations of GX 339–4, which span a smaller range in $\delta\nu_{\rm max}$ than the ones of Swift J1753.5-0127. Taken into account all observations again no clear correlation is evident.

Having a look at the ratio of the flux contributed by the disc blackbody component to the one coming for the Componized component in the soft (1 – 2 keV) band (the values are given in the last row of Table 3), we find that this ratio is below ∼7% for the two observations for which the characteristic frequencies are consistent within errors (observation of H 1743–322 and 2006 observation of Swift J1753.5−0127), while it is above 20% for those observations where we found $\delta\nu_{\rm max;1-2keV} < \delta\nu_{\rm max;4-8keV}$. In the case of XTE J1650–500 and XTE J1752–223, the ratio exceeds one hundred per cent, which means that the flux of the disc component contributes more than 50% of the total flux in the soft band. For XTE J1752–223 this high value might be attributed to the fact that the source is observed during outburst decay, but this is not true for XTE J1650–500 which was observed during outburst rise. In Fig.7 we show the flux ratio versus the absolute and relative difference in the characteristic frequency of the component with the highest characteristic frequency. Even ignoring the two data points with a flux ratio larger than one, there no clear correlation that a larger absolute or relative change of the characteristic frequency would be related to a larger flux ratio.

3.3 Covariance spectra

To investigate variability of spectral components we derived covariance spectra on long (segments of 270 s with 2.7 s time bins) and short (segments of 4 s with 0.1 s time bins) time scales (Fig. 8). The

Table 3. Spectral parameters

param.	GX 339/04	GX 339/09	Sw1753/06	Sw1753/12/1	Sw1753/12/2	XTE1650	XTE1752	H 1743
N_{dbb}	40922^{+15215}_{-13085}	10825^{+5996}_{-3448}	1526^{+676}_{-771}	3434^{+972}_{-1102}	5526^{+1511}_{-1630}	187432^{+17585}_{-14993}	62815^{+6523}_{-5511}	–
T_{in} [keV]	$0.202^{+0.013}_{-0.009}$	$0.223^{+0.014}_{-0.012}$	$0.213^{+0.033}_{-0.040}$	$0.270^{+0.010}_{-0.006}$	$0.257^{+0.014}_{-0.009}$	$0.275^{+0.004}_{-0.003}$	$0.234^{+0.003}_{-0.002}$	$0.001^{\natural}$
E_{coff} [keV]	7.6 ± 0.2	7.4 ± 0.2	> 9.3	7.2 ± 0.2	$7.3^{+0.1}_{-0.2}$	7.7 ± 0.4	$6.8^{+0.2}_{-0.1}$	$1.73^{+0.04}_{-0.02}$
E_{fold} [keV]	$17.8^{+6.5}_{-3.8}$	$19.8^{+5.6}_{-2.4}$	–	$15.1^{+3.9}_{-3.4}$	15.4 ± 2.2	$20.8^{+7.4}_{-5.1}$	$35.5^{+5.7}_{-4.6}$	$5.1^{+1.3}_{-0.8}$
N_{nthc}	$0.329^{+0.009}_{-0.014}$	$0.199^{+0.006}_{-0.010}$	> 0.06	$0.138^{+0.006}_{-0.009}$	$0.167^{+0.004}_{-0.008}$	$1.640^{+0.070}_{-0.072}$	$0.226^{+0.006}_{-0.005}$	$0.087^{+0.003}_{-0.002}$
Γ	1.65 ± 0.01	$1.53^{+0.03}_{-0.05}$	1.73 ± 0.03	$1.57^{+0.03}_{-0.07}$	$1.60^{+0.01}_{-0.06}$	$1.87^{+0.02}_{-0.03}$	1.77 ± 0.02	$1.03^{+0.03}_{-0.01}$
kT_e [keV]	$4.6^{+1.7}_{-0.7}$	$7.6^{+7.6}_{-2.2}$	> 9.5	$8.0^{+17.5}_{-3.0}$	$7.1^{+11.4}_{-1.6}$	> 6.1	> 7.8	$14.1^{+5.1}_{-1.4}$
χ^2/dof	46.7/76	48.3/76	54.2/79	92.6/79	91.0/79	83.7/79	114.9/79	75.0/78
$F_{dbb}/F_{pl}^{\dagger}$[%]	23.1	20.0	6.8	31.6	31.0	167.1	172.8	0

Notes:
†: ratio of the flux contributed by the disc emission to the one of the Comptonized emission in the 1 – 2 keV band
$^{\natural}$: value used as seed temperature in the NTHCOMP model (fixed)

covariance spectra have been fitted with the same model used for the averaged energy spectra in Section 3.2. We adjusted the binning of the response files to the number of bins present in the covariance spectra using the ftool RBNRMF. In the cases where 50 bins have been used (GX 339–4 and H 1743–322) the rebinding led to an artificial feature consisting of a spike and a trough-like structure at energies between 5.8 and 6.8 keV (the energy range of the Iron Kα emission). Hence, this energy range has been ignored in the fits of the covariance spectra. For both observations of GX 339–4 it is not possible to obtain formally acceptable fits as the data points stagger around the obtained best fit at energies below 2 – 2.5 keV. In the spectral fitting of all covariance spectra a systematic uncertainty of one per cent has been included.

The covariance spectra of XTE J1650–500 and XTE J1752–223 do not require a high-energy cut-off component to obtain acceptable fits. For these two observations the photon indices and inner disc temperatures obtained from the covariance spectra are larger than those obtained from the mean energy spectra.

For the remaining observations a comparison of the behaviour of the photon index and inner disc temperature between short and long term covariance spectra as well as between covariance and mean energy spectra can be found in Table 5.

The consistency of photon indices of short and long time scale covariance spectra of the 2004 observation of GX 339–4 and the 2006 observation of Swift J1753.5-0127 agrees with the results presented by Wilkinson & Uttley (2009). They also obtained a bigger photon index from the mean energy spectrum compared to the one obtained from covariance spectra for the 2006 observation of Swift J1753.5-0127. In the case of the 2004 observation of GX 339–4 Wilkinson & Uttley (2009) found a smaller photon index from the mean energy spectrum compared to the one obtained from covariance spectra, contrary to what we found. This difference can be related to the inclusion of a reflection component in the study of Wilkinson & Uttley (2009) that becomes obvious at higher energies covered by RXTE but inaccessible with *XMM-Newton*.

Apart form the observation of XTE J1650-500 and the October 2012 observation of Swift J1753.5-0127 the disc normalisation obtained from the long time scale covariance spectra are larger than the one obtained from the short time scale covariance spectra, although they all agree within their rather big error bars. In case of consistent photon indices, this higher disc blackbody normalisation indicates additional disc variability on long time scales (Wilkinson & Uttley 2009).

3.3.1 *Covariance ratios*

A model-independent way to compare variability on long and short time scales are covariance ratios, which we show in Fig. 9. The observations of GX 339–4, XTE J1752–223 and the 2006 and October 2012 observations of Swift J1753.5–0127 show a clear increase in the covariance ratio at energies below about one keV. Apart from the October 2012 observations of Swift J1753.5–0127 we found a higher disc blackbody normalisation for the long time scale covariance spectra in these observations, which is consistent with the increase found in the covariance ratios. This increase has been interpreted as a sign of additional disc variability on longer time scales by Wilkinson & Uttley (2009). In case of the October 2012 observation of Swift J1753.5–0127 we found a change of the photon index between short and long time scale covariance spectra which may explain why the additional long-term disc variability observed in the covariance ratio does not show up in a higher disc normalisation in the long time scale covariance spectrum. We also found significantly different photon indices for the short and long time scale covariance spectra of XTE J1752–223. As changes in the photon index indicate changes of the overall spectral shape, the difference in photon index may explain the increase of covariance ratio with increasing energy seen in XTE J1752–223.

4 DISCUSSION

At the beginning of this section we would like to summarise the main results:

- In Obs. 1, 2, 5, 6, 7, 8 the band limited noise component with the highest characteristic frequency shows a lower characteristic frequency in the soft band compared to the one observed in the hard band.
- In all these observations the ratio of the disc blackbody flux to the flux of the Comptonized component in the soft band exceeded ~10%. In Obs. 7 and 8 it even exceeds 100 per cent. In Obs. 3 and 4 the ratio is below 10 per cent.

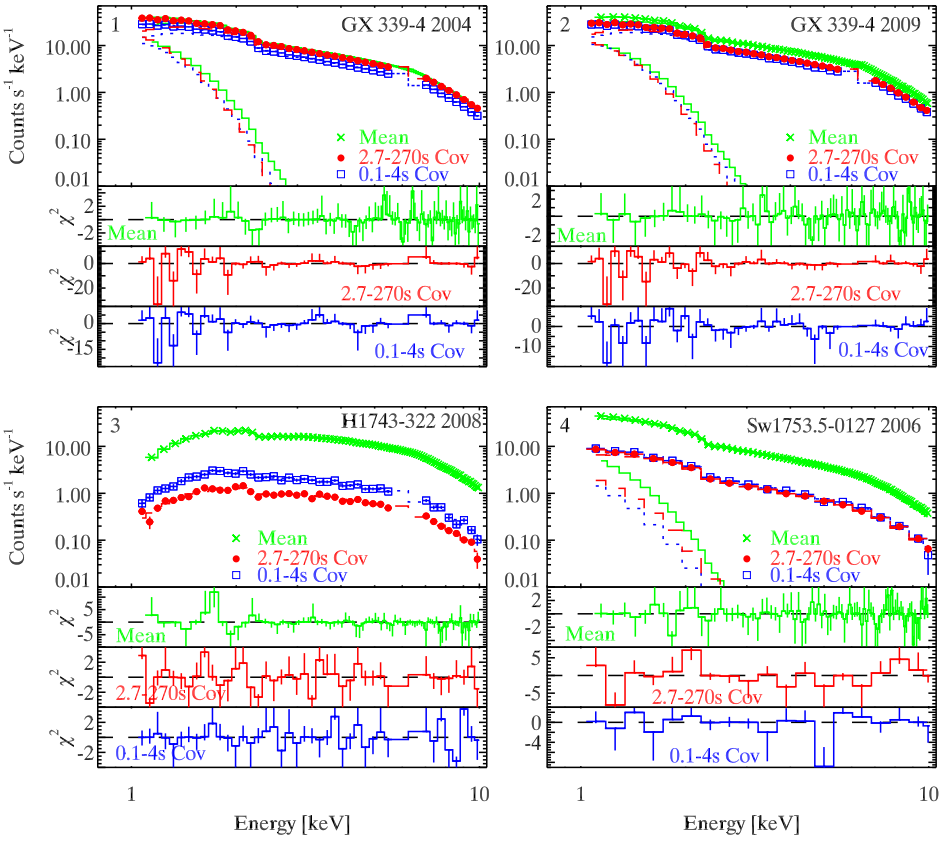

Figure 8. Mean energy spectra (green crosses) and covariance spectra on short (blue squares) and long (filled red circles) time scales for all eight observations. Best-fit model and individual components (disc blackbody and Comptonisation component) are indicated (dotted lines for short time scale covariance spectra; dashed lines for long time scale covariance spectra). In addition, χ^2 distributions for the fits of all three spectra are shown.

- In Obs. 1, 2, 3, 5 the rms spectrum is either flat or slowly decreasing with energy. Obs. 4 and 6 show a jump in variability around 4 – 5 keV, while variability remains rather constant at lower and higher energies. Obs. 7 and 8 show much lower variability in the 1 – 2 keV band compared to the rather constant variability above 2 keV.
- The covariance ratios of Obs. 1, 2, 4, 6, 8 show a clear increase at lower energies. In Obs. 7 and 8 the photon indices and inner disc temperatures obtained from the covariance spectra are larger than those obtained from the mean energy spectra. Obs. 1, 2, 5, 6 do not show a general correlation between spectral parameters obtained from covariance and mean energy spectra.

Our investigations of the characteristic frequency of the band limited noise in a hard and soft energy band revealed that for observations where the ratio of the disc blackbody flux to the flux of the Comptonized component in the soft band exceeded ~10%, the band limited noise component with the highest characteristic frequency shows a lower characteristic frequency in the soft band compared to the one observed in the hard band. The energy dependence of the characteristic frequency is more obvious at characteristic frequencies above 1 Hz in the hard band.

The energy dependence of the characteristic frequency observed in the 2004 observation of GX 339–4 and the 2006 observation of Swift J1753.5-0127 concur with the energy dependence found in a qualitative study of the PDS shape that was based on the same *XMM-Newton* observations (Wilkinson & Uttley 2009). This study of Wilkinson & Uttley also presented the increase of covariance ratios at lower energies and interpreted it as additional variability of the accretion disc relative to the power-law component at low frequencies (<1 Hz), while the soft band blackbody variations at frequencies above 1 Hz are probably mostly produced by X-ray heating caused by the reprocessing of Comptonized photons in the accretion disc.

In a study of XTE J1650-500 and XTE J1550-564, based on RXTE/PCA data, Gierliński & Zdziarski (2005) showed PDS in the ~2 – ~13 and ~13 – ~ 25 keV bands for different states. It is interesting to notice that for their LHS PDS of XTE J1650-500 the PDS of their hard band lies below the PDS of their soft band (i. e. the power in the hard band is smaller than the power in the soft band at the same frequency), while for the energy bands used here the soft band PDS lies below the hard band PDS (see Fig. 1). In addition to the PDS Gierliński & Zdziarski (2005) also showed rms spectra for different states. In their study of XTE J1650-500 and XTE J1550-

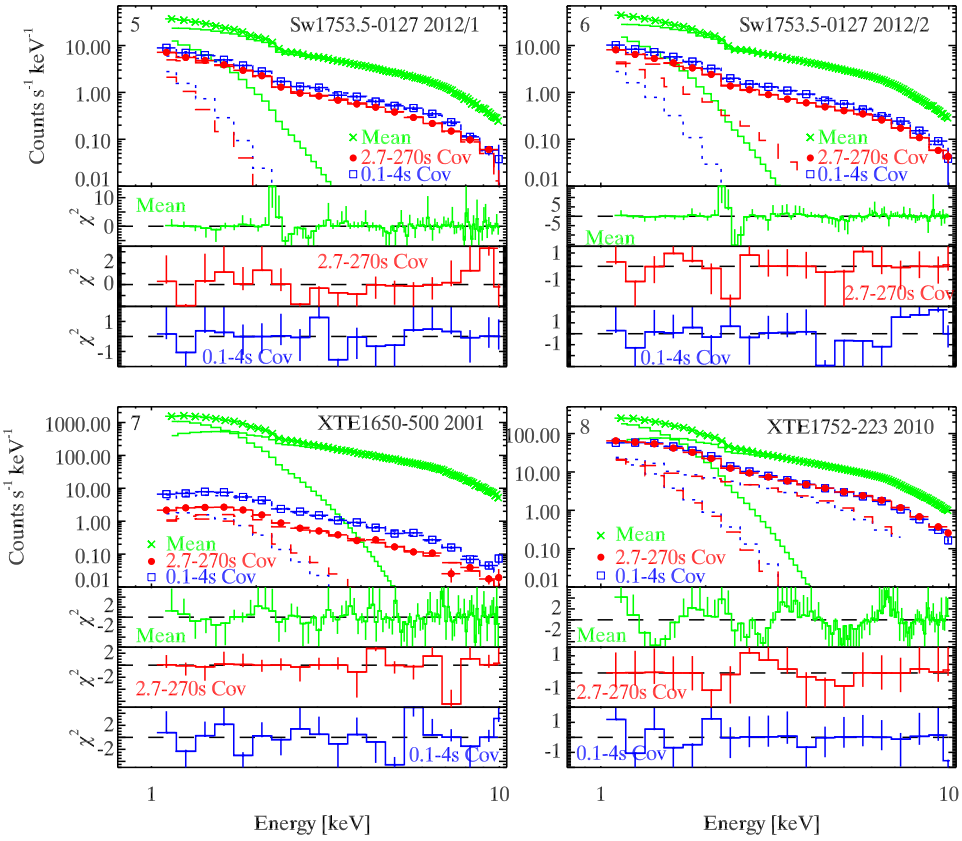

Figure 8. continued

564 they observed flat rms spectra and an rms slightly decreasing with increasing energy in the LHS. We found a similar behaviour in the observations of GX 339–4, H 1743–322, and the September 2012 observation of Swift J1753.5-0127. The behaviour of the rms observed in the remaining observations of Swift J1753.5-0127 corresponds to the one of the HIMS in the Gierliński & Zdziarski (2005) study.

The observed energy dependence of the characteristic frequency which is more obvious at characteristic frequencies above 1 Hz in the hard band can be either explained by variable seed photon input for the Comptonized photons in different energy bands (Gierliński & Zdziarski 2005) or by X-ray heating of the accretion disc caused by the reprocessing of Comptonized photons (Wilkinson & Uttley 2009). The variability properties observed in our study show characteristics of variability associated with Comptonized photons down to the lowest observed energies, i. e. that the PDS can be described by BLN and QPOs in all energy bands and that a power-law shape observed in the HSS when disc variability dominates in not needed. The energy dependence of the characteristic frequency suggests that the seed photon input for the Comptonized photons varies between different energy bands, as has been discussed in Gierliński & Zdziarski (2005) based on RXTE data. It is therefore expected that such an effect would become more obvious when the corona is cooled down and the electron temperature is getting lower. Thus the energy dependence becomes more obvious in narrower energy bands.

The presence of the energy dependence of the characteristic frequency can be interpreted within the picture where the photons in the soft and hard energy bands come from different locations in the system. A schematic sketch of this picture, which was also used in our recent studies (Yu & Zhang 2013; Stiele & Yu 2014), is given in Fig. 10. When the thermal disc component emerges in the soft band of *XMM-Newton* but does not dominate, a significant number of photons in the soft energy band will still come from the Comptonization component (originating either from an optically thin hot corona (see e. g. Esin et al. 1997) or from a jet flow (see e. g. Markoff et al. 2005)). However, the soft band photons should origin further away from the black hole than the hard band ones and thus suffer less up-scattering. This brings lower characteristic frequencies and softer energies together. The change of the characteristic frequency can be interpreted as a hint of a temperature gradient in the Comptonization component.

The observation that the energy dependence of the characteristic frequency is mainly observed at higher frequencies (>1 Hz) can be interpreted as a moving in of the inner disc radius during outburst evolution. In early outburst stages the disc ends far away from the black hole and the characteristic frequency, which is below 1 Hz, is consistent between both bands, since the photons in

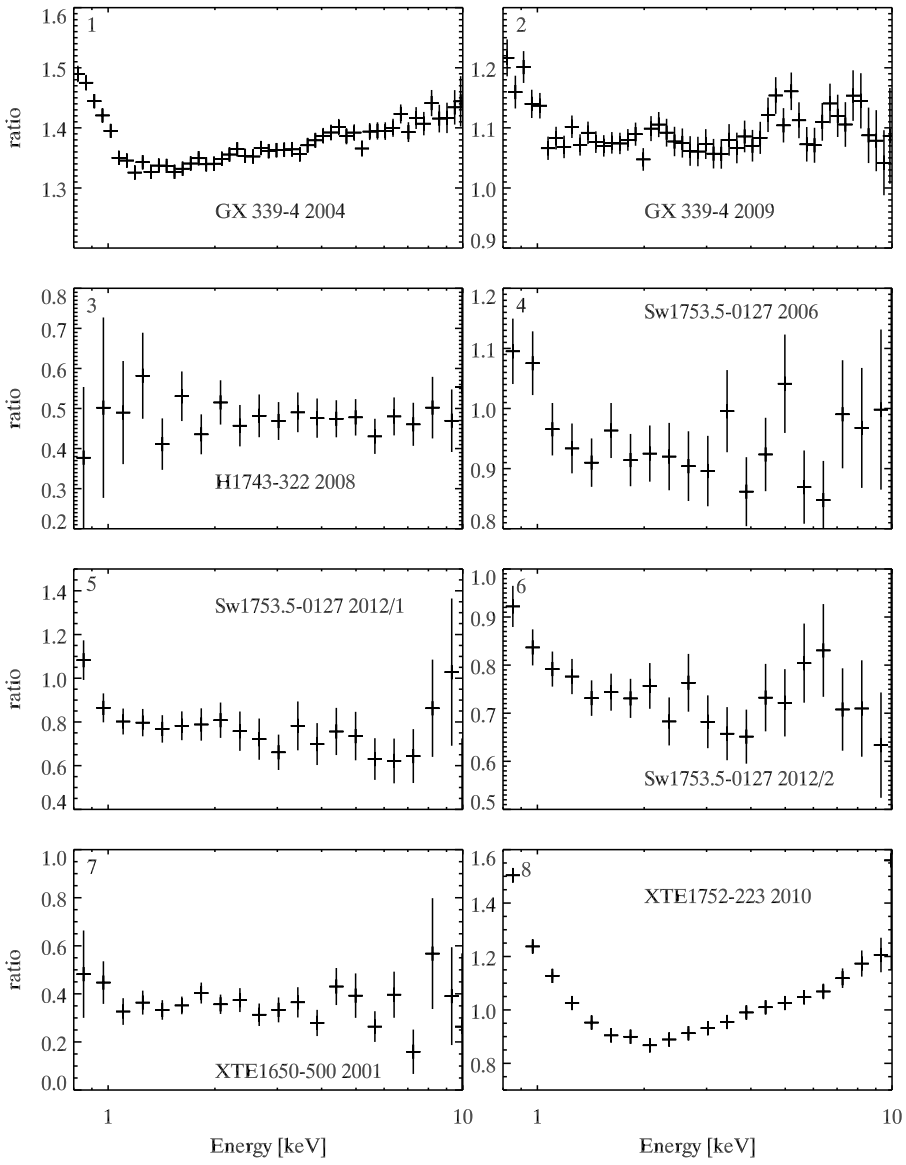

Figure 9. Covariance ratio of all eight observations.The ratios are obtained by dividing the covariance spectra obtained on longer time scales by those obtained on shorter time scales.

both bands experience a similar number of scatterings. With ongoing evolution of the outburst the boundary region between the disc and the Comptonizing corona moves inwards and the characteristic frequency as well as the contribution of the direct disc emission in the soft band increases (Ingram & Done 2011). Notice that the radius at which the cold disc ends may be not the radius at which the cold disc terminates (as assumed in the truncation disc model; e. g. Dubus et al. 2001; McClintock & Remillard 2006; Done et al. 2007), since a hot flow or corona would cover the innermost cold disc so the radius one determines from the cut-off frequency of the power-law noise would correspond to the radius to which the hot flow or corona extends (while the disc can reach down to the ISCO as assumed e. g. in Beloborodov 1999; Merloni & Fabian 2002; Miller et al. 2006; Reis et al. 2013).

Interpreting the energy dependence of the characteristic frequency by additional intrinsic disc variability at low energies is not a convincing alternative, as intrinsic disc variability contributes at low frequencies (Wilkinson & Uttley 2009) while the observed energy dependence of the characteristic frequency is more pronounced at frequencies above 1 Hz. In addition, the subsample of observations that show an increased covariance ratio at low energies does not agree with the subsample of observations that show the energy dependence of the characteristic frequency. We would like to point out that the additional disc variability on long time scales shows up only in the covariance spectra and ratios, but that there is no hint of an additional disc component in the PDS at low energies. As PDS fitting does not require any disc variability (see Sect. 3.1), we can exclude that the observed energy dependence of

Table 4. Parameters of covariance spectra

param.	GX 339/04	GX 339/09	Sw1753/06	Sw1753/12/1	Sw1753/12/2	XTE1650	XTE1752	H 1743
				short				
N_{dbb}	110485^{+27382}_{-31347}	17357^{+8237}_{-4697}	$653^{+104357}_{-569}$	$12876^{+459848}_{-11454}$	9763^{+96716}_{-7286}	152^{+275}_{-62}	846^{+145}_{-121}	–
T_{in} [keV]	$0.183^{+0.007}_{-0.002}$	0.205 ± 0.010	$0.198^{+0.092}_{-0.086}$	$0.173^{+0.040}_{-0.049}$	$0.179^{+0.043}_{-0.046}$	$0.314^{+0.058}_{-0.091}$	0.382 ± 0.012	$0.001^{\natural}$
E_{coff} [keV]	7.2 ± 0.2	> 0.01	> 6.0	$7.5^{+1.4}_{-1.2}$	> 5	–	–	$1.69^{+0.14}_{-0.20}$
E_{fold} [keV]	$19.7^{+4.1}_{-1.1}$	> 0.01	> 0.01	$5.6^{+16.6}_{-3.7}$	> 0.01	–	–	$2.5^{+0.3}_{-0.2}$
N_{nthc}	$0.324^{+37.254}_{-0.005}$	$0.117^{+0.004}_{-0.005}$	$0.013^{+0.001}_{-0.002}$	$0.036^{+0.003}_{-0.001}$	$0.048^{+0.004}_{-0.006}$	$0.021^{+0.007}_{-0.004}$	$0.071^{+0.005}_{-0.003}$	0.010 ± 0.002
Γ	$1.58^{+0.02}_{-0.03}$	1.52 ± 0.03	$1.68^{+0.03}_{-0.08}$	$1.68^{+0.05}_{-0.10}$	$1.75^{+0.03}_{-0.05}$	$2.37^{+0.09}_{-0.19}$	$2.08^{+0.03}_{-0.04}$	$1.00^{+0.46}_{-0.00}$
kT_e [keV]	$7.1^{+0.0}_{-1.5}$	$8.3^{+3.7}_{-1.8}$	> 5	> 3.4	> 5.6	> 5	> 5	< 21
χ^2/dof	109.7/31	111.6/33	22.8/12	7.4/12	14.9/12	28.0/14	4.4/8	32.5/33
				long				
N_{dbb}	272909^{+54522}_{-62781}	29555^{+6530}_{-7352}	6649^{+16426}_{-5371}	$28577^{+370948}_{-24309}$	6576^{+5856}_{-3258}	24^{+18}_{-9}	1124^{+208}_{-168}	–
T_{in} [keV]	$0.169^{+0.007}_{-0.005}$	$0.192^{+0.008}_{-0.005}$	$0.154^{+0.038}_{-0.018}$	$0.151^{+0.000}_{-0.035}$	$0.199^{+0.024}_{-0.017}$	$0.420^{+0.065}_{-0.075}$	0.361 ± 0.011	$0.001^{\natural}$
E_{coff} [keV]	$7.3^{+0.3}_{-0.2}$	> 0.01	> 12.0	> 9.8	> 0.01	–	–	< 1.6
E_{fold} [keV]	$22.1^{+5.0}_{-3.1}$	> 0.01	> 0.01	> 0.01	> 0.01	–	–	$2.4^{+1.0}_{-0.2}$
N_{nthc}	$0.442^{+0.011}_{-0.018}$	0.133 ± 0.002	0.011 ± 0.001	$0.034^{+0.001}_{-0.000}$	$0.021^{+0.002}_{-0.005}$	0.005 ± 0.002	$0.058^{+0.003}_{-0.002}$	$0.004^{+37.253}_{-0.001}$
Γ	$1.57^{+0.02}_{-0.03}$	$1.54^{+0.01}_{-0.03}$	$1.61^{+0.03}_{-0.06}$	$1.77^{+0.03}_{-0.04}$	$1.57^{+0.05}_{-0.27}$	$2.24^{+0.23}_{-0.29}$	$1.86^{+0.03}_{-0.02}$	$1.00^{+0.23}_{-0.00}$
kT_e [keV]	$8.2^{+4.3}_{-2.3}$	$7.0^{+4.3}_{-1.3}$	$9.2^{+72.2}_{-3.3}$	> 5.6	> 2.9	> 5	> 6.6	< 22
χ^2/dof	143.5/31	150.9/33	23.9/9	14.1/12	8.5/12	14.7/14	5.8/8	36.8/33

Notes:
$^{\natural}$: value used as seed temperature in the NTHCOMP model (fixed)

Table 5. Behaviour of photon index and inner disc temperature comparing parameters obtained from covariance spectra on both time scales and of parameters obtained form covariance spectra to those of mean energy spectra

param.	GX 339/04	GX 339/09	Sw1753/06	Sw1753/12/1	Sw1753/12/2	H 1743
			covariance to mean energy spectra			
Γ	smaller	agree	agree (s) smaller (l)	agree (s) bigger (l)	†	agree
T_{in}	smaller	agree (s) smaller (l)	agree	smaller	smaller	smaller
			short term to long term covariance spectra			
Γ	agree	agree	agree	agree	do not agree	agree
T_{in}	do not agree	agree	agree	agree	agree	agree

Notes:
†: For the October 2012 observation of Swift J1753.5-0127 the photon index obtained from the mean energy spectrum lies between the values obtained from the covariance spectra and agrees within error bars with the one obtained from long scale covariance spectrum.
(s), (l): short, long term scale covariance spectra, respectively
agree: short for: agree within error bars
Table should be read like this: For the 2004 observation of GX 339–4 the photon indices obtained from the long and short term covariance spectra are smaller than the one obtained from the mean energy spectrum.

the characteristic frequency is caused by underlying disc variability not taken into account properly during PDS fitting. Thus we prefer to interpret the energy dependence of the characteristic frequency to be caused by variable seed photon input for the Comptonized photons in different energy bands.

A challenge to our interpretation might be the observations of XTE J1650−500 and XTE J1752−223. In both observations the contribution of the disc emission to the overall emission in the soft band exceeds 50 per cent, and based on the results obtained in Stiele & Yu (2014) and Yu & Zhang (2013) we would expect that the sources are in the hard intermediate state. The fact that the signal-

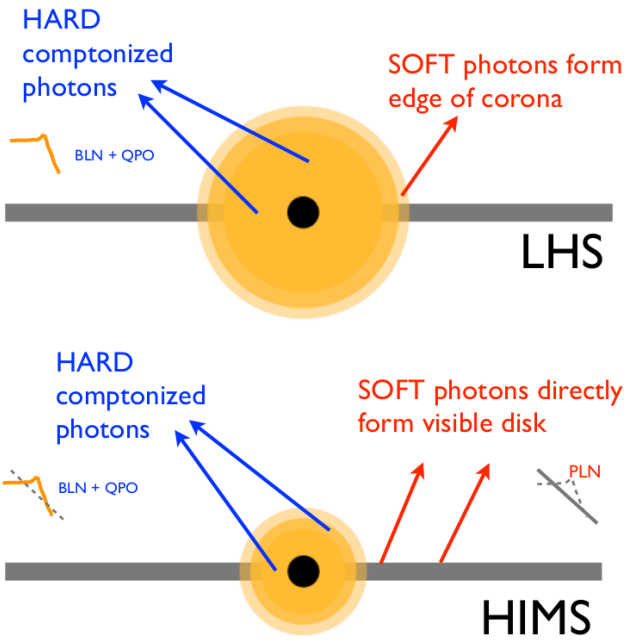

Figure 10. Schematic picture of the accretion geometry and the observed power spectral components obtained from our recent studies of black hole X-ray binaries during low hard state (upper panel) and around transition to the (hard) intermediate state (lower panel), see also Yu & Zhang (2013) and Stiele & Yu (2014).

to-noise ratio at higher energies is lower in these two observations compared to the other observations used in this study cannot explain why the contribution of the disc emission to the overall emission in the soft band exceeds 50 per cent, as taking the error bars on the spectral parameters into account does not affect the flux ratio to always exceed 50 per cent. We notice that for these two observations the variability amplitude in the softest band is lower than the variability amplitude at higher energies. Furthermore, fitting of the covariance spectra of these two sources does not require a high-energy cut-off and the photon indices and inner disc temperatures obtained from the covariance spectra are larger than those obtained from the mean energy spectra. For XTE J1752−223 this discrepancy can be explained by the fact that XTE J1752−223 is observed during outburst decay returning to the LHS, while the results of Stiele & Yu (2014) and Yu & Zhang (2013) are based on the evolution from the hard to the soft state. In the case of XTE J1650−500, it is more difficult to find an explanation as the source is observed during outburst rise when it evolves from the LHS to the HSS. A possible explanation can be that in this source the contribution of the disc emission to the soft band is in general higher than in those sources studied by Stiele & Yu (2014) and Yu & Zhang (2013). A thorough investigation of this possibility as well as a detailed study of the differences between outburst rise and decay will be the targets of future studies. Please notice that in these two observations the signal-to-noise ratio at higher energies is lower compared to the other observations used in this study. However, the lower signal-to-noise ratio cannot explain why the contribution of the disc emission to the overall emission in the soft band exceeds 50 per cent.

Regarding the absence of correlations between the characteristic frequencies in different energy bands and between the characteristic frequency and spectral parameters, it is mainly the data points of GX 339–4 with well constraint parameters that do not agree with possible trends seen in the remaining data points with bigger uncertainties. Higher quality data that would allow to constrain the characteristic frequency more precisely would be helpful to foster the absence of correlations.

In conclusion, the energy dependence of the break frequency of the band-limited noise component supports a picture that the power spectra in black hole X-ray binaries depend on which spectral components we are looking at. Energy-resolved timing observations can be sensitive enough to trace not only the accretion geometry by detecting power-law noise as evidence of the emergence of a disc component but can also probe the properties of the corona from studies of the band-limited noise break frequency. In this work we provide evidence that the energy dependence of the characteristic frequency may be used to probe the extension of the corona.

ACKNOWLEDGMENTS

We would like to acknowledge useful discussions with Jon Miller, Mike Novak, Diego Altamirano, Omer Blaes and Tomaso Belloni. This work makes use of software tools provided by Simon Vaughan. This work was supported by the National Natural Science Foundation of China under grant No. 11073043, 11333005, and 11350110498, by Strategic Priority Research Program "The Emergence of Cosmological Structures" under Grant No. XDB09000000 and the XTP project under Grant No. XDA04060604, by the Shanghai Astronomical Observatory Key Project and by the Chinese Academy of Sciences Fellowship for Young International Scientists Grant.

References

Belloni T., Hasinger G., 1990, A&A, 227, L33
Belloni T., Psaltis D., van der Klis M., 2002, ApJ, 572, 392
Belloni T., van der Klis M., Lewin W. H. G., van Paradijs J., Dotani T., Mitsuda K., Miyamoto S., 1997, A&A, 322, 857
Belloni T. M., 2010, in T. Belloni ed., Lecture Notes in Physics, Berlin Springer Verlag Vol. 794 of Lecture Notes in Physics, Berlin Springer Verlag, States and Transitions in Black Hole Binaries. p. 53
Belloni T. M., Motta S. E., Muñoz-Darias T., 2011, Bulletin of the Astronomical Society of India, 39, 409
Belloni T. M., Stella L., 2014, Space Sci. Rev., 183, 43
Beloborodov A. M., 1999, ApJ, 510, L123
Cao X., Yu W., 2009, ApJ, 690, 1363
Capitanio F., Belloni T., Del Santo M., Ubertini P., 2009, MNRAS, 398, 1194
Casella P., Belloni T., Stella L., 2005, ApJ, 629, 403
Cassatella P., Uttley P., Maccarone T. J., 2012, MNRAS, 427, 2985
Churazov E., Gilfanov M., Revnivtsev M., 2001, MNRAS, 321, 759
Cui W., Heindl W. A., Rothschild R. E., Zhang S. N., Jahoda K., Focke W., 1997, ApJ, 474, L57
Done C., Gierliński M., Kubota A., 2007, A&ARv, 15, 1
Dubus G., Hameury J.-M., Lasota J.-P., 2001, A&A, 373, 251
Esin A. A., McClintock J. E., Narayan R., 1997, ApJ, 489, 865
Gierliński M., Zdziarski A. A., 2005, MNRAS, 363, 1349
Houck J. C., Denicola L. A., 2000, in N. Manset, C. Veillet, & D. Crabtree ed., Astronomical Data Analysis Software and Systems IX Vol. 216 of Astronomical Society of the Pacific Confer-

ence Series, ISIS: An Interactive Spectral Interpretation System for High Resolution X-Ray Spectroscopy. p. 591
Ingram A., Done C., 2011, MNRAS, 415, 2323
Kirsch M. G. F., Schönherr G., Kendziorra E., Freyberg M. J., Martin M., Wilms J., Mukerjee K., Breitfellner M. G., Smith M. J. S., Staubert R., 2006, A&A, 453, 173
Kolehmainen M., Done C., Díaz Trigo M., 2011, MNRAS, 416, 311
Leahy D. A., Elsner R. F., Weisskopf M. C., 1983, ApJ, 272, 256
Lyubarskii Y. E., 1997, MNRAS, 292, 679
Markoff S., Nowak M. A., Wilms J., 2005, ApJ, 635, 1203
McClintock J. E., Remillard R. A., 2006, Black hole binaries. pp 157–213
McHardy I. M., Arévalo P., Uttley P., Papadakis I. E., Summons D. P., Brinkmann W., Page M. J., 2007, MNRAS, 382, 985
Merloni A., Fabian A. C., 2002, MNRAS, 332, 165
Miller J. M., Fabian A. C., Wijnands R., Reynolds C. S., Ehle M., Freyberg M. J., van der Klis M., Lewin W. H. G., Sanchez-Fernandez C., Castro-Tirado A. J., 2002, ApJ, 570, L69
Miller J. M., Homan J., Steeghs D., Rupen M., Hunstead R. W., Wijnands R., Charles P. A., Fabian A. C., 2006, ApJ, 653, 525
Miyamoto S., Kitamoto S., Iga S., Hayashida K., Terada K., 1994, ApJ, 435, 398
Mostafa R., Mendez M., Hiemstra B., Soleri P., Belloni T., Ibrahim A. I., Yasein M. N., 2013, MNRAS, 431, 2341
Motta S., Muñoz-Darias T., Casella P., Belloni T., Homan J., 2011, MNRAS, 418, 2292
Muñoz-Darias T., Motta S., Belloni T. M., 2011, MNRAS, 410, 679
Reis R. C., Miller J. M., Reynolds M. T., Fabian A. C., Walton D. J., Cackett E., Steiner J. F., 2013, ApJ, 763, 48
Remillard R. A., McClintock J. E., 2006, Annual Rev. of A&A, 44, 49
Stiele H., Motta S., Muñoz-Darias T., Belloni T. M., 2011a, MNRAS, 418, 1746
Stiele H., Munoz-Darias T., Motta S., Belloni T., 2011b, PoS(Texas 2010)032
Stiele H., Yu W., 2014, MNRAS, 441, 1177
Uttley P., McHardy I. M., 2001, MNRAS, 323, L26
Walton D. J., Reis R. C., Cackett E. M., Fabian A. C., Miller J. M., 2012, MNRAS, 422, 2510
Wijnands R., Homan J., van der Klis M., 1999, ApJ, 526, L33
Wilkinson T., Uttley P., 2009, MNRAS, 397, 666
Wilms J., Allen A., McCray R., 2000, ApJ, 542, 914
Yu W., Zhang W., 2013, ApJ, 770, 135
Zdziarski A. A., Gierliński M., Mikołajewska J., Wardziński G., Smith D. M., Harmon B. A., Kitamoto S., 2004, MNRAS, 351, 791
Zdziarski A. A., Johnson W. N., Magdziarz P., 1996, MNRAS, 283, 193
Zhang W., Jahoda K., Swank J. H., Morgan E. H., Giles A. B., 1995, ApJ, 449, 930
Życki P. T., Done C., Smith D. A., 1999, MNRAS, 309, 561

This paper has been typeset from a TEX/ LATEX file prepared by the author.